communications earth & environment

Article

https://doi.org/10.1038/s43247-024-01919-1

Homo erectus adapted to steppe-desert climate extremes one million years ago

Julio Mercader[1,2,3,4] ✉, Pamela Akuku[3,5,6], Nicole Boivin[2,7], Alfredo Camacho[8], Tristan Carter[9,10], Siobhán Clarke[1], Arturo Cueva Temprana[2], Julien Favreau[9], Jennifer Galloway[4], Raquel Hernando[3,11], Haiping Huang[4], Stephen Hubbard[4], Jed O. Kaplan[4], Steve Larter[4], Stephen Magohe[4,12], Abdallah Mohamed[13], Aloyce Mwambwiga[1,14], Ayoola Oladele[1], Michael Petraglia[7,15,16], Patrick Roberts[2], Palmira Saladié[3,5,17], Abel Shikoni[13], Renzo Silva[4,18], María Soto[19,20], Dominica Stricklin[1], Degsew Z. Mekonnen[21,22], Wenran Zhao[4] & Paul Durkin[8] ✉

Questions about when early members of the genus *Homo* adapted to extreme environments like deserts and rainforests have traditionally focused on *Homo sapiens*. Here, we present multidisciplinary evidence from Engaji Nanyori in Tanzania's Oldupai Gorge, revealing that *Homo erectus* thrived in hyperarid landscapes one million years ago. Using biogeochemical analyses, precise chronometric dating, palaeoclimate simulations, biome modeling, fire history reconstructions, palaeobotanical studies, faunal assemblages, and archeological evidence, we reconstruct an environment dominated by semidesert shrubland. Despite these challenges, *Homo erectus* repeatedly occupied fluvial landscapes, leveraging water sources and ecological focal points to mitigate risk. These findings suggest archaic humans possessed an ecological flexibility previously attributed only to later hominins. This adaptability likely facilitated the expansion of *Homo erectus* into the arid regions of Africa and Eurasia, redefining their role as ecological generalists thriving in some of the most challenging landscapes of the Middle Pleistocene.

Debate has long centered on when the genus *Homo* acquired the adaptability to thrive in extreme environments like deserts and rainforests[1–3]. Traditionally, only *Homo sapiens* was thought capable of sustained occupation in such ecosystems[2,3], with archaic hominins seen as restricted to narrower ranges[4,5]. However, biogeochemical, palaeoenvironmental, and archaeological evidence suggests that early *Homo* had the ability to adapt to diverse[6] and unstable environments from the East African Rift floor[7] and Afromontane[8] areas as early as two million years ago. Here, we present a multidisciplinary analysis of geological, palaeontological, archaeological, chemical, and palaeobotanical data from Engaji Nanyori in Tanzania's Oldupai Gorge, revealing that *Homo erectus* adapted to shifting hyperarid landscapes one million years ago—well before our species emerged. This adaptive profile, marked by resilience in arid zones, challenges assumptions about early hominin dispersal limits and positions *H. erectus* as a versatile generalist and the first hominin to transcend environmental boundaries on a global scale.

Earth system models[4,5] predict that *Homo habilis* and *Homo ergaster* (African *Homo erectus*) were highly sensitive to environmental variability, possessed a restricted ecological range, and were vulnerable to eccentricity-modulated precessional cycles in palaeoclimate. This sensitivity has been taken as evidence that these species lacked the broad adaptability needed to thrive in diverse ecosystems, reinforcing their classification as environmental specialists[4–6], widely thought to have predominantly occupied mosaic environments comprising forests, woodlands, and grasslands. As these hominins ventured into regions with extreme annual precipitation—whether very low or very high—survival would have required specialized adaptive capabilities that did not fully emerge until the appearance of *Homo sapiens*, when more generalised strategies enabled a global ecological scope[1–3]. This perspective, however, is informed by fragmentary data from key evolutionary periods, it has limited palaeoecological resolution at the local level, and comes from a very small number of scattered palaeoanthropological sites. Further, there lies an additional research challenge in distinguishing a hominin species' ecological niche—defined as the full range of environmental conditions it could exploit—from its cultural flexibility with which it responds to environmental changes. This paper reexamines the adaptability of African *Homo erectus* and argues that their ecological niche was not shaped by abiotic factors like climate alone, but also by their capacity to overcome physiological and cognitive challenges. By integrating these aspects, we question the prevailing view of African *Homo erectus* as an ecological specialist and offer a more nuanced understanding of their

A full list of affiliations appears at the end of the paper. ✉e-mail: mercader@ucalgary.ca; paul.durkin@umanitoba.ca

adaptability. This perspective expands our conception of early hominin capabilities, indicating that the development of generalist strategies preceded *Homo sapiens* and occurred much earlier than previously believed, beginning with at least the Middle Pleistocene Transition (MPT, 1.2–0.8 Ma).

To examine how climatic fluctuations affected the ecological range, dispersal patterns, and technologies of early *Homo*, we undertook interdisciplinary research at a key early hominin locality in Tanzania's equatorial zone, Engaji Nanyori[9,10], Oldupai Gorge, Bed III[11]. Here we present large datasets from newly excavated contexts, a comprehensive sedimentary stratigraphy, and a chronological framework of precise absolute dates that contextualize the position of *Homo erectus* remains found in the 1960s[12,13]. Utilizing a multi-proxy approach, our research indicates that the region surrounding Oldupai Gorge experienced semidesert conditions spanning the first half of the MPT. The vegetation characteristic of these semideserts, including taxa such as *Ephedra* spp., is presently found only in areas located thousands of kilometers to the north, along the margins of the Sahara, and extending into Arabia. This evidence leads us to propose that early hominins were able to adapt to and persist within hyperarid environments, demonstrating a broader ecological plasticity than previously understood. Our analysis, incorporating data on plant communities, wildfires, butchered faunal remains, and abundant stone tools, reveals a behavioural response to aridity characterised by persistent focality in land use and provisioning. In response to severe aridity during the MPT, hominins mitigated risk by strategically inhabiting fluvial landscapes, repeatedly occupying the same locality over millennia. Their exploitation of faunal and lithic resources near river confluences highlights a stable, adaptive strategy to the arid conditions prevailing in the Eastern African steppe deserts during this period.

Results

Fluvial dynamics, sedimentary stratigraphy, and chronology

During the deposition of Bed III (1.2–0.9 million years ago), the geography of the eastern Serengeti underwent substantial changes due to tectonic and climatic processes[11,14–17]. Normal faulting associated with rifting led to alterations in the position of the Oldupai sedimentary basin and the fluvial drainage networks within it[11] (Fig. 1, Supplementary Note 1). As a result, rivers shifted their courses towards the east and north, traversing saline, calcic, and alkaline floodplains[11,14], as shown by the precipitation of analcime and calcretes (Supplementary Fig. 1). Palaeolake Oldupai experienced drying episodes, indicated by fluctuations in its water levels, the presence of hiatuses, and geochemical markers of drought[15–17](Supplementary Fig. 2). These drying phases also led to the formation of desert red beds[18,19] resulting from the oxidation of iron-bearing sediments (Fig. 1, Supplementary Figs. 3 and 4).

A fluvial confluence formed to the north of Engaji Nanyori during the MPT, marking one of the exceedingly rare artifact/fossil sites from this stage. The type locality for Bed III[9,10] contains evidence for two coalescing watersheds with vastly different biomes: the volcanic highlands to the southeast and the Serengeti plains to the west (Fig. 2, Supplementary Fig. 5). Channel-belt deposits are differentiated into two types by sediment provenance, orientation, and distribution (Supplementary Fig. 6). Perennial and ephemeral streams left a complex sedimentological record of the changing environments, expressed in packages of six facies (Fig. 1, Supplementary Note 1, Supplementary Fig. 2, Fig. 3): volcaniclastic conglomerate (facies 1), mottled red mudstone (facies 2), reddish brown mudstone (facies 3), fine-to-coarse sandstone (facies 4), light-gray-to-pink siltstone (facies 5), and gray mudstone (facies 6). These facies represent meandering fluvial channels ~1 m deep/~20 m wide and associated floodplains, which are expressed in three stratigraphic units: 3–1, 3–2, and 3–3 (Fig. 1). Within unit 3–2, the deposits of three distinct channel belts have been recently identified: A, B, and C (Fig. 1, Supplementary Note 1), characterised by sandy-to-gravelly point-bar and fine-grained abandoned-channel deposits. The oldest is C (equivalent to the 'lower coarse gray sand' of Leakey[10]), consisting of channel-belt deposits amalgamated vertically and laterally. The deposits of channel-belt B are 125 m wide and characterized by iron-stained gravels (Leakey's 'fine-grained ferruginous sand'[10]). Channel-belt A is the youngest and is dominated by cross-stratified gravelly sandstones (Kleindienst's trenches A and B[9]) that fine upward – these finer deposits yielded *Homo erectus* fossils (Olduvai Hominid, OH34)[12], 0.5 m below Leakey's siltstones with 'pits and furrows (Supplementary Fig. 4B)[10], and about 5 m southeast from the current research area (Fig. 1, Supplementary Fig. 7).

At the study site, Bed III accumulated 10 m of sediment over the course of 300,000 years[20] (Fig. 1A). Bed III sediments are readily identifiable by their prominent brick-red color located 3.5 m above Tuff IID (upper Bed II; Fig. 1A, B, Supplementary Figs. 2 and 8). Conflicting age estimates for key marker Tuff IID[21] have been resolved with a new $^{40}Ar/^{39}Ar$ age of 1.332 ± 0.020 Ma (2σ) from a nearby outcrop in the eastern palaeobasin that is physically and geochemically correlated with both Engaji Nanyori (Fig. 4, Supplementary Figs. 8–10) and the western gorge[22] (see Methods, Supplementary Table 1, https://doi.org/10.20383/103.0901). The new radiometric age and correlation establish a consistent basin-wide age for Tuff IID. Using our new age from Tuff IID as a chronostratigraphic anchor, we constrain previous models[20] and suggest an age of 1.19 ± 0.06/0.07 Ma (1σ) for the base of Bed III (Fig. 4). This absolute date is essential amidst the very sparse ages available for Bed III. It not only clarifies previous uncertainties and discrepancies[21] but also extends the chronology of lowermost Bed III to the onset of the MPT, from a previous estimate of 1.14 ± 0.07 Ma[20], while placing *Homo erectus*[12], for the first time, in the middle of Bed III (stratigraphic unit 3-2) at 0.99 ± 0.06/0.07 Ma (1σ) (Figs. 1B and 4). This revised age estimate for hominin OH34 is based on its stratigraphic position, as determined within the geological column, and supported by age-depth modelling.

Ecological degradation during the middle Pleistocene transition

In regions where extensive evapotranspiration in closed basins limits freshwater availability, barren lands often emerge, leading to the formation of steppe deserts or semidesert environments[23–25]. Within the context of Engaji Nanyori, evidence of *Homo erectus*' adaptability to extreme and highly variable mid-Pleistocene climates becomes apparent amidst arid conditions, reduced plant cover, and frequent ecological disturbances due to fire. Fossil pollen analysis, from a semidesert plant community characterized by a considerable proportion of gymnosperms compared to angiosperms (10:1), with Gnetales being the dominant order (Fig. 5), reveals the presence of at least six species of xeric ephedroid shrubs (Supplementary Table 2, Fig. 6, Supplementary Note 2). Notably, the pollen record is predominantly composed of Ephedripites pollen (Fig. 5E, F), primarily produced by *Ephedra*, a genus known for its drought-resistant characteristics indicative of peri-Saharan ecosystems[26–28].

To our knowledge, this discovery marks the first and southernmost occurrence of *Ephedra* outside the Saharo-Arabian zone, indicating that, in response to increased aridity during the MPT, Oldupai Gorge, at 3°S, was enveloped by Saharo-Sindian vegetation, extending over 1000 km southward from its current 3°N limit[27–30] (Fig. 5). To further explore the palaeoenvironment of the East African Rift System during the MPT and evaluate the prevalence of hyperarid conditions, we applied the same palaeoclimate-vegetation modelling framework as recent Earth system studies[4,5]. While lower resolution models may suggest that the hominin habitat suitability index exceeded 0.5[4,5], our field-based palaeoenvironmental data synthesis provides abundant evidence for high aridity, including signs of lake desiccation, saline/alkaline soils, desert red-bed formation, and increased wildfire activity at Oldupai Gorge. Furthermore, using their palaeoclimate data from the pCESM-3Ma simulations and the BIOME4 model, we generated high-resolution (1 km) regional biome projections (Fig. 7, Supplementary Fig. 11). The results indicate that the MPT was characterised by alternating phases of mesophytic and xerophytic plant communities, with the most arid conditions occurring during MIS 30, particularly around 1.043 million years ago. These simulations reveal a notable expansion of semidesert ecosystems into equatorial Africa during the MPT, particularly in the area between Oldupai Gorge and the southeastern part of Lake Victoria, where semideserts replaced present-day

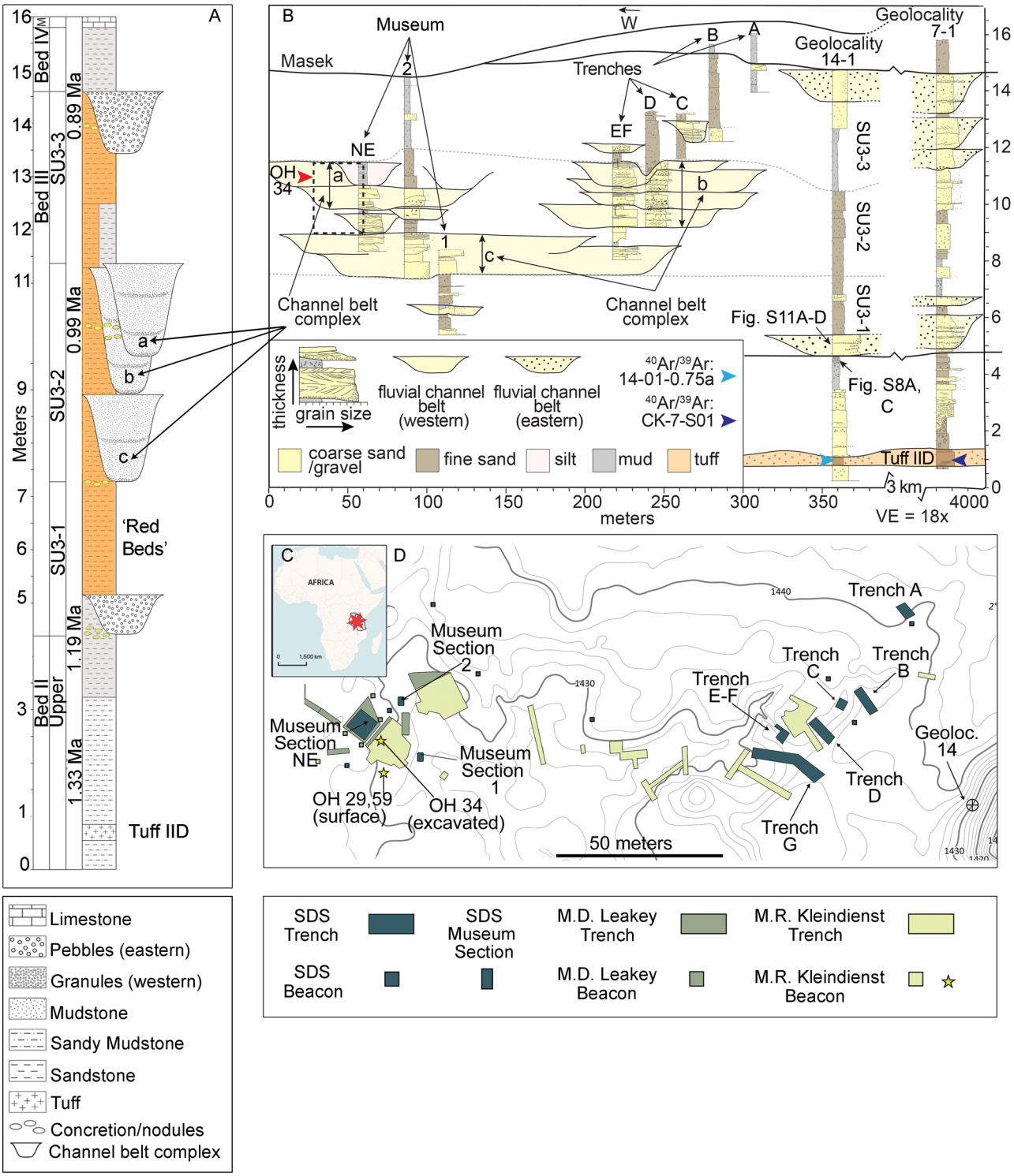

Fig. 1 | Engaji Nanyori stratigraphy, sedimentary architecture, placement of excavated materials, and site map. A The stratigraphic diagram displays the lithology, location of channel-belt complexes, and stratigraphic units found in Beds II, III, and IV. Additionally, it illustrates the stratigraphic positioning of *Homo erectus* remains from the 1960s (Olduvai Hominid no. 34)[12,13]. M Masek. **B** Stratigraphic cross section at Engaji Nanyori spanning from the Leakey Museum (West) to geological locality no. 14 (Juma's Korongo Cliff) and Emurutoto (geological locality no. 7) in the East. The vertical extent of this study is from Tuff IID (Bed II) to the Masek Beds, with a focus on the channel-belt deposits from Bed III. The approximate vertical location of Olduvai Hominid 34 is indicated by a red arrow. SU stratigraphic unit. **C**, **D** Location in Eastern Africa and site map showing the position of archaeological trenches excavated by Kleindienst in 1962[9], Leakey in 1970[10], and our team in 2022.

woodlands and grasslands. Additionally, the entire Turkana basin is represented as a true desert, devoid of vegetation and surface water.

The analysis of stable carbon isotopes in herbivore tooth enamel indicates a diet dominated by C_4 grasses (Supplementary Table 3), which are adapted to high irradiance temperatures (Supplementary Fig. 12), contrasting with the mixed C_3–C_4 photosynthetic pathway observed in the Oldupai basin during the early Pleistocene[31]. Additionally, the examination of floodplain soils from facies 2 shows phytoliths from woody shrubs and

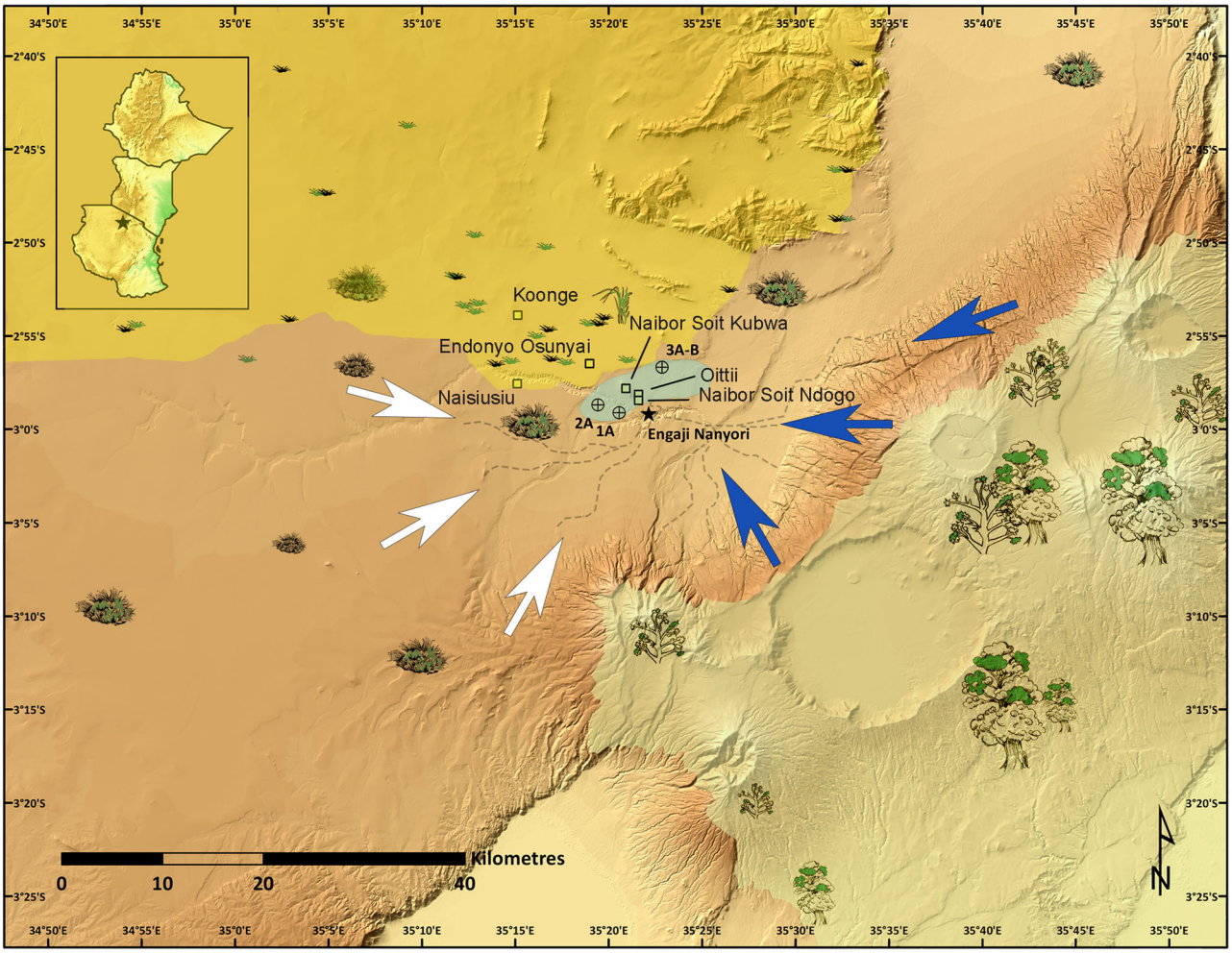

Fig. 2 | Regional plant landscape reconstruction based on palaeobotanical, geological, and isotopic proxies. The dominant plant group at Oldupai Gorge during the initial Middle Pleistocene Transition was the gymnosperms. The volcanic highlands (lower right, pale green shading) were home to conifers, while the eastern Serengeti was covered with ephedroid shrubs, monocots, and C_4 grasses. Engaji Nanyori (star symbol) sat at the confluence of eastern (blue arrows) and western sourced (white arrows) streams. Drill sites[16] are shown as a target symbol. The quartzite sources used by Acheulean hominins at Engaji Nanyori are marked as squares.

monocots (Supplementary Figs. 13 and 14). These were deposited under conditions of high evaporation and carbonate precipitation leading to the nucleation of zeolites[32] on phytoliths and the fossilization of tap roots (Supplementary Fig. 15) resembling those of *Ephedra* species[28]. Furthermore, the presence of mid-chain normal alkanes (n–C_{23}) (Supplementary Fig. 16) suggests the existence of aquatic herbaceous plants near active meandering channels.

The sedimentary record from Engaji Nanyori provides an account of past wildfires, discernible through molecular and microscopic markers. Analysis of saturated hydrocarbons reveals branched and cyclic alkanes with a distinct odd-even carbon pattern (Fig. 8, Supplementary Note 3, Supplementary Figs. 16 and 17, Supplementary Table 4). The extraordinary predominance of short-chain, even carbon-numbered homologs in the n-alkane distributions is an indication of incomplete burning of biomass, a common feature of wildfire residue[33]. During charring, long-chain n-alkanes undergo major reduction, leading to short-chain, even carbon-numbered n-alkanes (m/z 85) typically at C_{18} or C_{16}. The co-occurrence of branched and cyclic alkanes (dominant peaks in m/z 127, 141/m/z 68, 82, respectively) exhibiting a pronounced odd/even carbon predominance further supports the notion that heat-induced processes contribute to the observed n-alkane patterns (Supplementary Fig. 17). Another line of evidence reinforcing pyrogenic origin is the ratio of unsubstituted polycyclic aromatic hydrocarbons (PAH) to their alkylated counterparts (P/∑MP). For example, the prevalence of phenanthrene, a primary constituent in the formation of PAHs, compared to alkylated methylphenanthrenes, helps establish the presence of combustion-derived PAHs throughout the site, with average ratios ranging from 1.03 to 1.43, confirming combustion events. Additionally, the ratio of fluoranthene (Fl) to pyrene (Py) compounds, with an average of 0.67, is a signature of pyrogenic PAHs, adding to the evidence of past fire in the area. Lastly, regional-scale fire activity is confirmed by the abundance of sedimentary microscopic charcoal, with fluctuating fire regimes of varying intensity (Supplementary Fig. 18, Supplementary Table 5).

Responses to drought

In the hyperarid basin of Bed III, hominin activity chiefly focused on a location where fresh, flowing water would have been more frequent due to the presence of two river systems with radically different drainage basins. Precipitation in either basin would have provided river discharge and increased the likelihood of available water over a single drainage system. The strategic choice of habitat around river focal spots accumulated evidence of a long history of stone tool production to process animal carcasses. During the 1960s and 1970s, Engaji Nanyori yielded a wealth of reworked artifacts and fossils excavated from high-energy contexts[9,10], including channels, point bars, and subaqueous dunes, all typical of facies 3. Previous work interpreted these remains as evidence that hominins camped by flowing water. (We

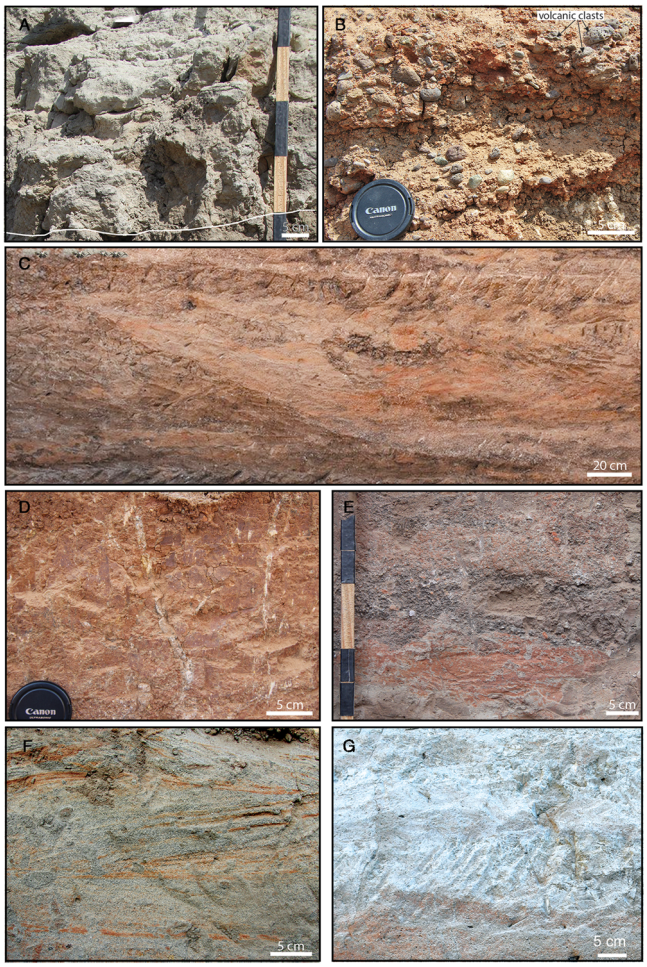

Fig. 3 | Outcrop and trench-face photographs of key geological features at Engagi Nanyori. A Tuff IID exposed at JK Cliff (Supplementary Fig. 8). **B** Volcanic-clast conglomerate of lower channel-belt deposits in 14–1. **C** Channel-belt deposit margin in Museum trench no. 1-NE indicating channel depths of ~1 m. **D** Calcareous rhizoliths in reddish mudstone typical of Bed III floodplain deposits. **E** Granular sandstone typical of western basement derived sediment source (see Supplementary Fig. 6E, F). **F** Cross-stratified channel-belt 2 sandstones from Trench D. Paleocurrent directions were derived from the dip direction of foresets. **G** Structureless white-to-pinkish siltstone of channel-belt A in Museum trench no. 1 -NE.

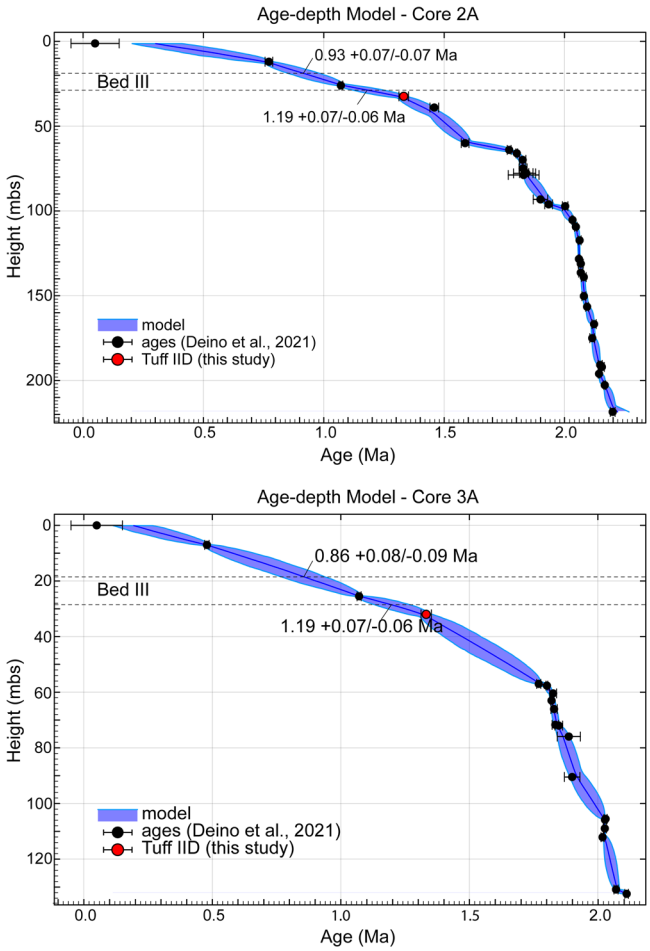

Fig. 4 | Refined age-depth model for lake drill cores 3 A and 2A[20] incorporating new age estimates: Tuff IID from Emurutoto (1.332 ± 0.020 Ma 2σ), Base of Bed III (1.19 ± 0.07/0.06 Ma, 95% CI), and Olduvai Hominid 34 (*Homo erectus*) (0.99 ± 0.07/0.05 Ma 95% CI). The new Tuff IID date (red circle) is plotted 3.5 m below Bed III as the equivalent horizon in Cores 2 A and 3A[20]. Utilising previously published ages[20] and the Chron.jl Bayesian age-depth model code, we incorporate the new Tuff IID age to model age-depth relationships in both cores. The model estimates ages for the base and top of Bed III at a 95% CI. The mean age for the base of Bed III from both cores is 1.19 ± 0.07/0.06 Ma, differing from previous models which estimated it at 1.14 Ma[20]. The age of the top of Bed III is estimated at 0.93 for Core 2 A and 0.86 ± 0.08/0.09 Ma for Core 3 A, consistent with previous models[20]. The age of *Homo erectus* fossils, as per the position we established for them in the geological column, is estimated at 0.99 ± 0.07/0.05 Ma.

have reconstructed the active channel dimensions as measuring 1 m deep and 20 m wide.) However, we show here that the original habitat preferred by hominins and the primary source of all cultural materials were the sinuous pond-like environments of facies 5, developed laterally to the stream by abandoned river channels following their avulsion. These were common on the western side of Engaji Nanyori, which hosts the richest archaeological accumulation and served as central points for both previous (Kleindienst[9], Leakey[10]) and new work. These preferred pond habitats were once widespread but were preserved only exceptionally due to the continual reworking and erosion caused by the migration of new channels across the landscape. Unlike the secondary, high-energy contexts reported by Kleindienst[9] and Leakey[10], the muddy siltstone from the abandoned channels we present is low energy. This sedimentary environment (Supplementary Figs. 3 and 4B) was filled by fine-grained sediments from subsequent overbank flow during high discharge events, burying hundreds of tools and animal bones in primary position and excellent conditions, with no preferential orientation of stones or fossils (Supplementary Fig. 19). Massive to weakly bedded and well-sorted sediments preserved multiple palaeosurfaces, inclusive of the 'pits and furrows' (Supplementary Fig. 4B) for which Leakey built a museum in the 1970s[10]. The intricate depressions, furrows, and runnels (Supplementary Fig. 4B) were small pits and traction marks closely reminiscent of those found in the Kilwa Group sandstones[34], attributed to the daily movements of invertebrates over wet mud preserved as trace fossils.

Homo erectus brought in large amounts of quartzite slabs to the abandoned channels and pond edges of facies 5, while sourcing phonolite and basalt from the riverbed cobbles (Fig. 3B). Geochemical fingerprinting shows that the bulk of rock provisioning to make tools targeted metamorphic outcrops restricted to a corridor two to thirteen km tangentially away along the fluvial confluence (Fig. 2, Supplementary Figs. 20–23, Supplementary Note 4). Four layers (I-IV) were distinguished, based on sedimentological, stratigraphic, and archaeological criteria (Supplementary Figs. 24–29). Engaji Nanyori's stone toolkits are from the Acheulean complex (Fig. 9), boasting dense clusters[9,10] (legacy + herein reported ≥22,000 pieces over >300 m^2), and for the first time bridging the local cultural trajectories of early Pleistocene hominins at Oldupai Gorge such as *Homo habilis* and *Paranthropus boisei* (Bed I–II, 2.0–1.3 Ma), with species like *Homo erectus* from the Middle Pleistocene (Bed III–IV: 1.2–0.9 Ma)[10].

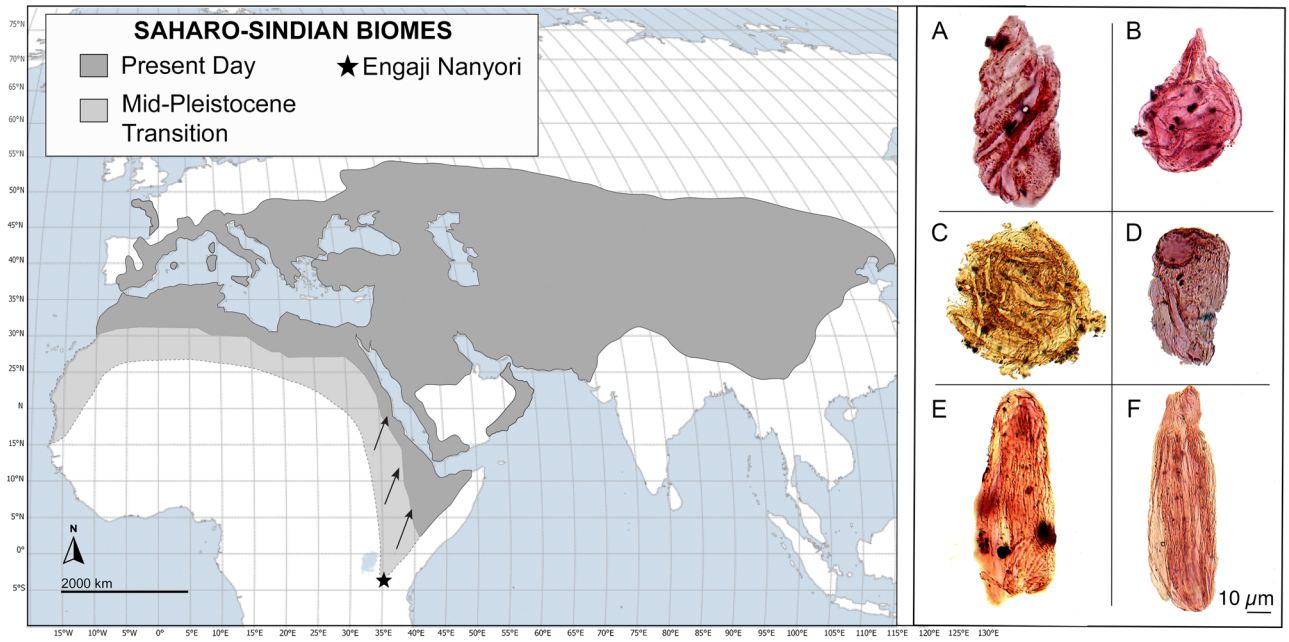

Fig. 5 | Geographical extent of the Ephedraceae and Saharo-Sindian biomes during recent times[29] and their hypothesized extent during the Middle Pleistocene Transition in Africa. Key pollen types. Star symbol shows the location of Engaji Nanyori. Base map created by Renna Truong, Spatial and Numeric Data Services within Libraries and Cultural Resources at the University of Calgary, on January 22, 2024, using ESRI technology. Selected pollen: **A** *Gnetaceaepollenites clathratus* (Sample: Engaji Nanyori 2017, trench B: IIIA; preparation R-3986-15/OTC, England finder coordinates: T22/2). **B** *Elateroplicites spp.* (Sample: Engaji Nanyori 2017, trench B: IB; preparation R-3986-14/OTC, England Finder coordinates: S40/1). **C** *Gnetaceaepollenites diversus* (Sample name: Engaji Nanyori 2017, trench B: IB; preparation R-3986-14/OTC, England Finder coordinates: R8/2). **D** *Steevesipollenites multilineatus* (Sample name: Engaji Nanyori 2017, trench B: IB; preparation R-3986-14/OTC, England finder coordinates: L18/4). **E** *Ephedra* spp. (Sample name: Engaji Nanyori 2017, trench A: IV; preparation R-3986-12/OTC; England finder coordinates: L23/4). **F** *Ephedra* spp. (Sample name: Engaji Nanyori 2017, trench B: IIIa; preparation R-3986-15/OTC, England Finder coordinates: M18/1).

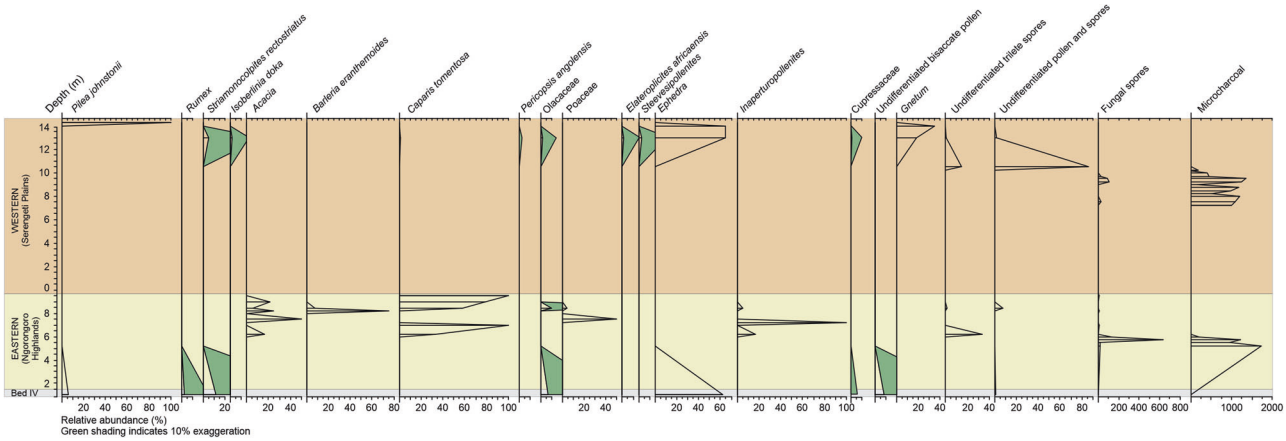

Fig. 6 | Summary pollen diagram showing vegetation groups. Eastern versus Western sourced sediments.

Facies 5 registers complete knapping sequences through hard percussion, as attested by cortical flakes, hammerstones, and diffuse bulbs (Supplementary Note 5), showing on-site lithic reduction. Of six stone exploitation methods (Supplementary Table 6–8), bifacial orthogonal, unipolar longitudinal, and bifacial centripetal dominated.

An intra-regional principal component analysis (PCA) of sites representing diverse hominin habitats, subsistence strategies, and key technological markers (Supplementary Fig. 30, Supplementary Tables 9–17) shows continuity between Engaji Nanyori and earlier Oldowan and Acheulean industries. When considering the entire knapping sequence, PCA demonstrates a close technical alignment with these sites (PC1-2 = 98.62% of the variance), particularly in core reduction strategies (PC1-2 = 83.70% of the variance), reflecting a shared technological framework. However, Engaji Nanyori exhibits a marked divergence in tool types, characterized by a higher proportion of retouched tools (burins, denticulates, and scrapers: PC1-2 = 82.43% of the variance) This increased representation of retouched tools, presumably used for butchery-related tasks, suggests that Engaji Nanyori functioned as a specialized site for resource processing and exploitation. This pattern of behaviour indicates that while *Homo erectus* maintained consistent knapping strategies across sites, they developed specialized tools to optimize subsistence activities in dryland niches.

The abundance of anthropogenically-accumulated animal bones suggests a successful, repeated utilization of the Engaji Nanyori locality by *Homo erectus* for primary and immediate access to axial and appendicular parts of prime adult bovids weighing <300 kg. The large quantities of animal

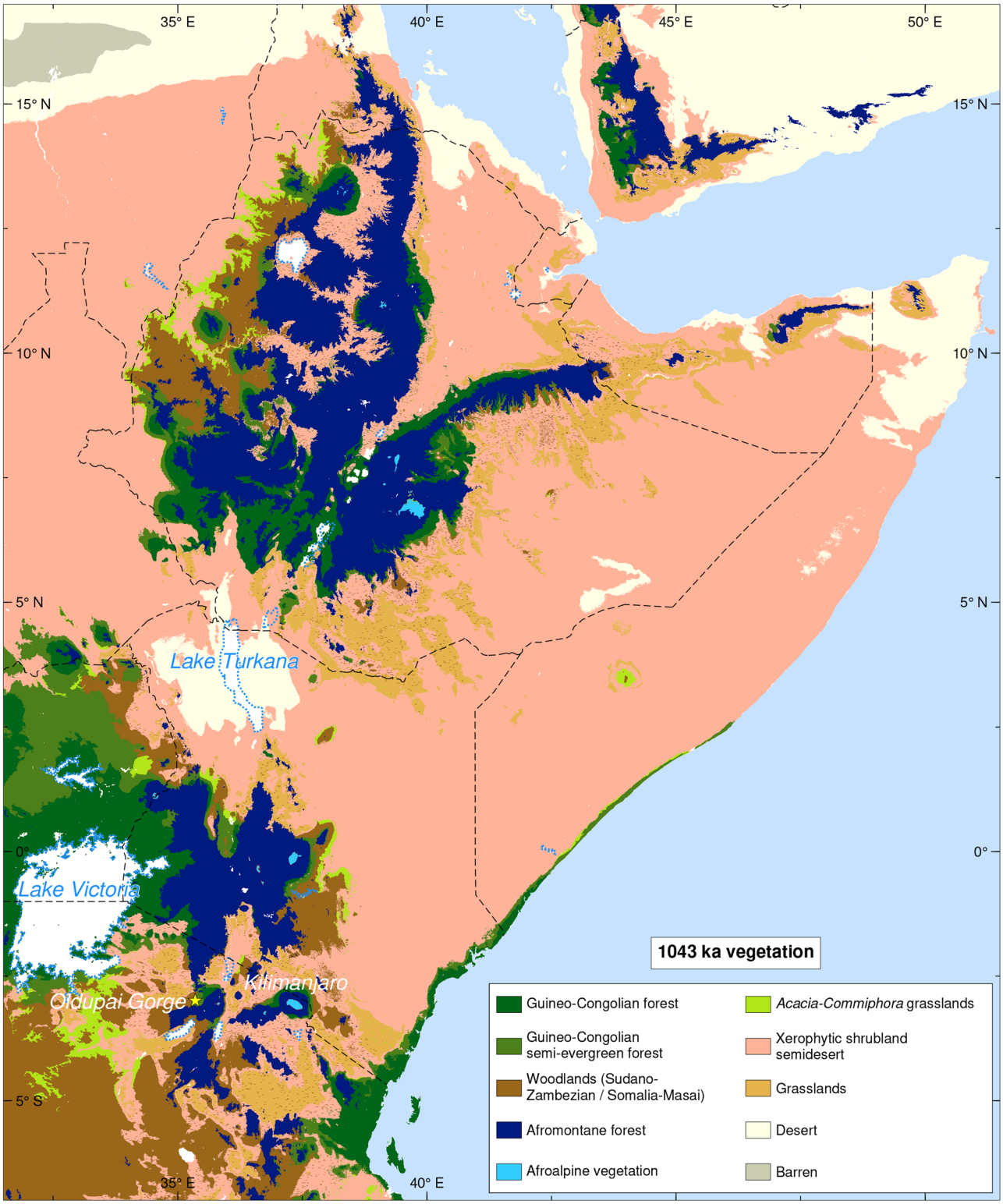

Fig. 7 | Vegetation map of the East African rift system at 1043 ka. Biomes are simulated using the BIOME4 global vegetation model driven by the pCESM.3 Ma palaeoclimate simulation.

bones (legacy + this paper ≥43,000 specimens over >300 m^2)[35–37] also demonstrate a persistent history of site use. The three-dimensional coordinates of excavated lithics and bones are positively correlated between them (Supplementary Table 18, Supplementary Fig. 28, Supplementary Note 6). That humans were the main predator and accumulator of animal remains is independently indicated by low levels of carnivore bone destruction and scarce tooth marks. Meat was intensively butchered (Fig. 10), Supplementary Figs. 31–37), with bones supporting abundant cut marks indicative of defleshing, skinning, and disarticulation. Marrow extraction is inferred from anthropogenic percussion pits and notches, associated with fresh fractures. Over half the fossils in the present study were taxonomically identifiable and revealed a low diversity assemblage heavily dominated by bovids (Supplementary Note 7, Supplementary Tables 19–23). The faunal remains include aquatic (Crocodylidae, Hippopotamidae) and open habitat

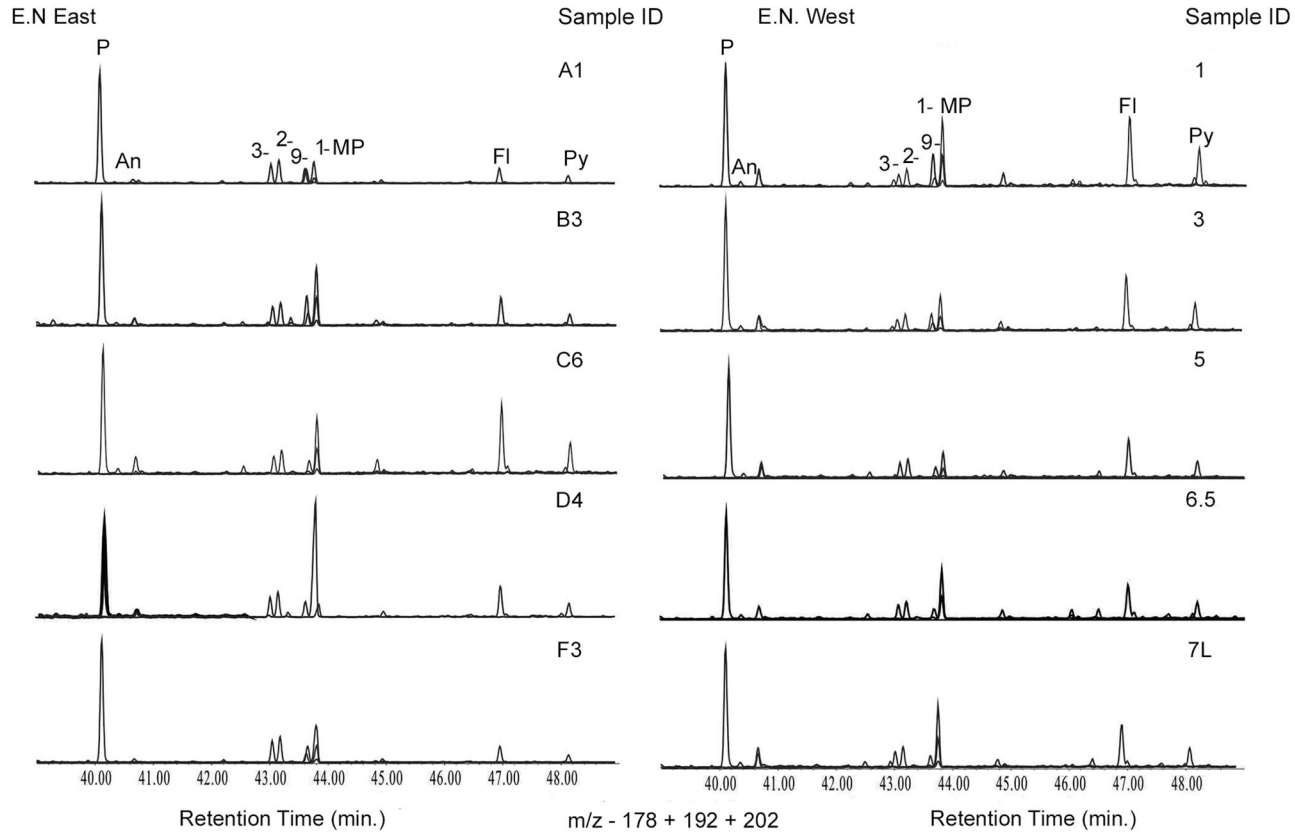

Fig. 8 | Overlaid ion chromatograms of mass over charge (m/z) 178, 192, and 202, illustrating the distribution of phenanthrene, methylphenanthrenes, fluoranthene, and pyrene in samples from Engaji Nanyori East and West. P phenanthrene, MP methylphenanthrenes, Fl fluoranthene, Py pyrene. An anthracene. The vertical axis represents relative abundance relative to the amount of sample injected in the instrument. To calculate concentrations, we use an internal standard.

taxa (Reduncini, Antilopini, Equidae). The water-dependent taxa are migratory or resilient denizens of ponds at times of drought, such as turtles and catfish.

Discussion

Range expansion and dispersal into the Saharo-Sindian zone

Palaeoclimate and vegetation model simulations[4,5] suggest that environmental conditions in northern Tanzania may have been moderately favorable for hominin occupation during MIS 30. The multi-proxy, field-based palaeoenvironmental reconstructions for the Oldupai region we present here do not support those simulations, and instead imply that conditions were characterized by extreme dryness. Biome models[4,5] overestimate the extent of woodlands, as we find little evidence for this vegetation in the biogeochemical sequences we analyzed. Furthermore, during MIS 30 Oldupai Gorge is characterized by lake desiccation, saline/alkaline soils, desert red-bed formation, and increased wildfires. Under such environmental conditions, the landscape was dominated by xerophytic ephedroid shrublands and would not have been ecologically suitable for woodlands. Despite the challenges posed by drylands, they likely played a crucial role in conditioning early human behaviour, technology, dispersals, and ecological expansions through Africa, the Levant, and Arabia. The new datasets from Engaji Nanyori underpin the study's conclusion that *Homo erectus* exhibited far greater adaptability to diverse ecologies than previously understood, with a capacity to persistently occupy extreme environments. Hominins showed a discerning and empirical understanding of their surrounding ecology through a combination of adaptive foraging strategies, tool use, environmental exploitation, and resource management practices tailored to their specific ecological context. Engaji Nanyori stands as the earliest example of African *Homo erectus* adapted to the encroaching aridity and high climatic variability of the initial MPT period. Based on the sedimentation time scale of the three-channel belts comprising the palaeoanthropological and archaeological remains, spanning 1000 to 10,000 years each[38], we can infer a prolonged cyclicity of human occupation of northern Tanzania's steppe deserts. Regular use of ecosystems prone to recurrent disruptions suggests a longstanding strategy of flexible habitat selection. This strategy likely derives its adaptive advantage from a reorganization of resource utilization prompted by environmental degradation and fragmentation. It prioritizes the establishment of camps near river confluences and emphasizes the importance of ponds for accessing water resources in challenging environments, rather than relying solely on changes in stone technology. Engaji Nanyori's Acheulean represents the earliest occupation of the Saharo-Sindian ecoclimatic zone, one of the largest and most diverse regions linking East Africa with North and West Africa, along with the Arabian Peninsula. The acquired ability to reside in marginal habitats provided the foundation for the remarkable adaptability that characterized *Homo* during the MPT, and probably made possible a widespread dispersal of *Homo erectus* into new, diverse, and extreme ecosystems across Eurasia. Engaji Nanyori indicates a paradigm shift concerning the understanding of the global settlement and ecological distribution of *Homo erectus*.

Methods

Geochemical characterization of geological samples

See https://doi.org/10.20383/103.0901 Supplementary Table 1 (Electron Microprobe Analysis conditions in the setup tab).

$^{40}Ar/^{39}Ar$ dating

All analytical work was performed at the University of Manitoba using a multi-collector Thermo Fisher Scientific ARGUSVI mass spectrometer, linked to a stainless-steel Thermo Fisher Scientific extraction/purification

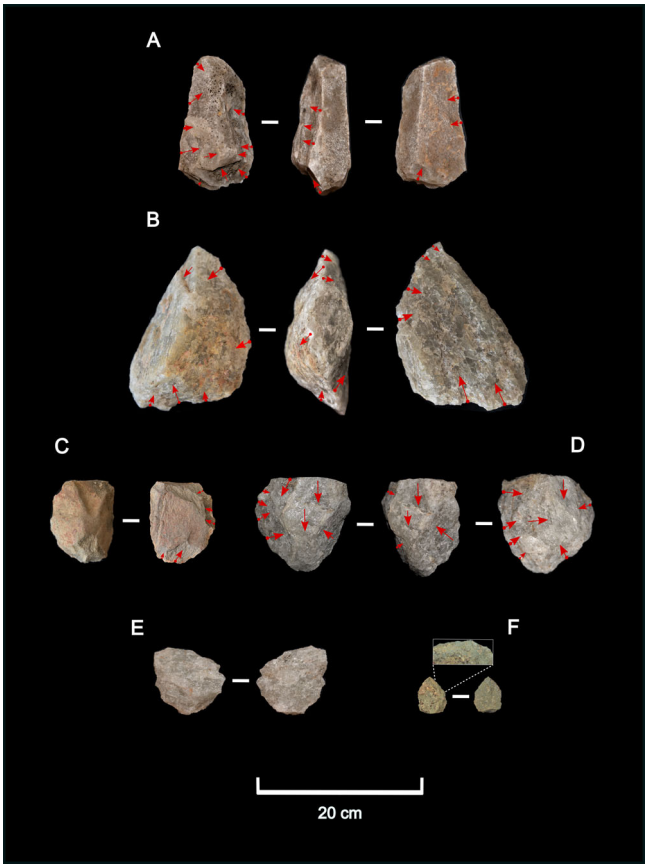

Fig. 9 | Selected stone tools from Engaji Nanyori. A Specimen no. 3713, quartzite Large Cutting Tool from Layer I. **B** Specimen no. 2486, quartzite Large Cutting Tool from Layer III. **C** Specimen no. 890, basalt cleaver-like tool from Layer IV. **D** Specimen no. 2262, quartzite bifacial centripetal core from Layer III. **E** Specimen no. 2318, quartzite denticulate from Layer III. **F** Specimen no. 1197, phonolite dihedral side scraper from Layer IV.

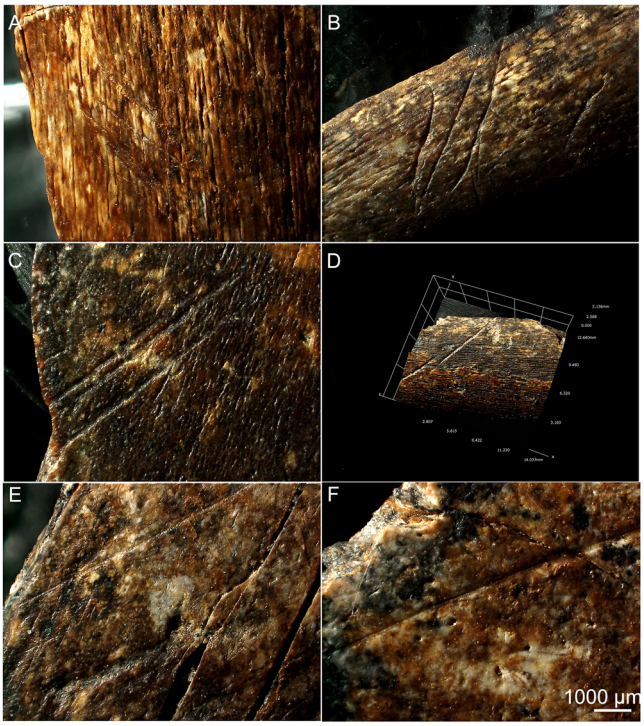

Fig. 10 | Evidence of bovid butchery by *Homo erectus*: bone cutmarks. A Oblique, parallel cutmarks on the anterior cortical surface of long bone; specimen ID: 192. E.N. Museum trench no. 1, Layer IV. **B** Oblique cutmark on long bone fragment; specimen ID 321. E.N. Museum trench no. 1, Layer IV. **C** Oblique, parallel cutmarks on long bone fragment; specimen ID 881. E.N. Museum trench no. 1, Layer IV. **D** 3-D profile of oblique and longitudinal cutmarks on the long bone fragment, specimen ID 952. E.N. Museum trench no. 1, Layer IV. **E** Oblique cut mark on long bone fragment; specimen ID 191. E.N. Museum trench no. 1, Layer IV. **F** Transversal cut mark on long bone fragment; specimen ID 54. E.N. Museum trench no. 1, Layer IV.

line and Photon Machines (55 W) Fusions 10.6 CO2 laser. Argon isotopes were measured using the following configuration: ^{40}Ar (H1; 1 ×1013 Ω resistor), ^{39}Ar (AX; 1 × 1013 Ω resistor), ^{38}Ar (L1; 1 × 1013 Ω resistor), ^{37}Ar (L2; 1 × 1013 Ω resistor) and ^{36}Ar (compact discrete dynode [CDD]). The sensitivity for argon measurements is ~6.3 × 1017 moles/fA as determined from measured aliquots of Fish Canyon Sanidine[39,40]. Standards and unknowns were placed in 2 mm deep wells in 18 mm diameter aluminum disks, with standards placed strategically so that the lateral neutron flux gradients across the disk could be evaluated. Planar regressions were fit to the standard data, and the ^{40}Ar/^{39}Ar neutron fluence parameter, J, interpolated for the unknowns. All specimens were irradiated in the Cadmium-lined, in-core CLICIT facility of the Oregon State University TRIGA reactor. The duration of irradiation was 3 hours and using the Fish Canyon sanidine (28.201 Ma)[40]. The astronomically calibrated Alder Creek rhyolite sanidine (1.18342 ± 0.00069 Ma)[41] was used as a secondary standard. Eight of the ten analyses (Table S1) yield an age of 1.181 ± 0.002 Ma (2 õ; MSWD = 3.52) relative to Fish Canyon sanidine. Irradiated samples were placed in a Cu sample tray, with a KBr coverslip, in a stainless-steel high vacuum extraction line and baked with an infrared lamp for 24 hours. Single crystals were either fused using the laser for one minute, and reactive gases were removed after ~1 mins by a JANIS cryocooler at ~−120 °C, an NP-10 SAES getter at room temperature, and a GP50 getter (C50 ST101 alloy) at 450 °C prior to being admitted to an ARGUSVI mass spectrometer by expansion. Five argon isotopes were measured simultaneously over a period of six minutes. Measured isotope abundances were corrected for extraction-line blanks, which were determined before every sample analysis.

Detector intercalibration (IC) between the different Faraday cups was monitored (in Qtegra) every three days by peak hopping ^{40}Ar. The IC factor between H1 and the CDD was measured with the unknowns by online analysis of air pipettes (IC values can be found in Supplementary Table 1 and https://doi.org/10.20383/103.0901). A value of 295.5 was used for the atmospheric ^{40}Ar/^{36}Ar ratio[42] for the purposes of routine measurement of mass spectrometer discrimination using air aliquots, and correction for atmospheric argon in the ^{40}Ar/^{39}Ar age calculation. Corrections are made for neutron-induced ^{40}Ar from potassium, ^{39}Ar and ^{36}Ar from calcium, and ^{36}Ar from chlorine[43–45]. Data collection and reduction were performed using Pychron. The decay constants used were those recommended by Min and others[46].

Molecular markers

Approximately 30 g of pulverized sample was soxhlet extracted with DCM:MeOH (93:7) for 72 h. The extracted organic material (EOM) was rotary-evaporated to a minimum volume and transferred to a graduated measuring cylinder. A known aliquot was removed and evaporated to dryness under a steady stream of nitrogen and weighed. Internal standards (cholestane-d4, adamantane-d16, squalane, naphthalene-d8, phenanthrene-d10, and 1,1-binaphthyl) were added to the remaining EOM based on the calculated sample dry weight. Aliphatic and aromatic hydrocarbons were fractionated on a silica column and eluted with pentane and isopropyl alcohol, respectively. For quality control purposes a solvent blank was included in the protocol, and one sample was run in duplicate.

Aliphatic and aromatic hydrocarbon fractions were analyzed using an Agilent 7890B Gas Chromatograph (GC) coupled to an Agilent 5977 A Mass Spectrometer (MS). GC analysis was performed using an HP-5MS

capillary column (30 m × 0.25 mm × 0.25 µm), 1 µl sample injected in splitless mode, injector temperature 250 °C, helium carrier gas at a constant flow rate of 1.0 ml/min. The GC oven temperature was initially held at 40 °C for 5 minutes and heated at a rate of 4 °C/min to 325 °C, then held for 15 minutes. The mass spectrometer was operated in electron ionization (EI) mode with an electron energy of 70 eV, running in simultaneous full scan (50–550 mz) and selected ion monitoring (SIM) modes.

Stable carbon and oxygen isotopic analyses

Samples from the buccal edge were collected using a diamond-tipped Dremel. Processing took place at the Applied Geochemistry group - Isotope Science Laboratory, Department of Earth, Energy and Environment, University of Calgary, Canada. Pure carbonate mineral species are analyzed by continuous flow isotope ratio mass spectrometry using a Thermo Finnigan GasBench® coupled to a DeltaVPlus®. A weighted sample equal to ~0.300 mg of pure calcite is weighed into a 12 mL Labco Exetainer (p/n: 038 W). The exetainers are loaded into a horizontal rack, uncapped. Approximately 200 µL of specially prepared anhydrous phosphoric acid is then carefully injected just inside the neck of the Exetainer. Because of the horizontal orientation, the acid remains near the vial neck in a small droplet, separated from the sample at the bottom of the vial. Vials are kept horizontal, capped, and flushed with UHP Helium for 10 minutes at a flow rate of ~70 ml/min. The vials are then turned vertically, allowing the acid droplet to run down to the bottom of the vial and react with the sample. Vials are then placed in the heated block of the GasBench at 25 °C and left to react for specified times (minimum of 5 h for calcite). The evolved CO_2 headspace is then sampled automatically by the gas bench using a 50 µL sample loop and inlet to the ion source of the mass spectrometer for analysis of $^{13}C/^{12}C$ and $^{18}O/^{16}O$ ratios. The headspace of each vial is sampled six times by loop injection. The first peak is discarded, and the 06_gb-delta_carbs subsequent 5 injections are acquired. If the first peak is >30 V, the subsequent five injections are automatically diluted by a factor of ~3:1 by the software.

Selected internal lab reference materials were run at the beginning and end of each set of samples and are used to normalize the data as well as correct for any instrument drift. These internal lab standards are periodically calibrated against international reference materials to assure accuracy to the Vienna Peedee Belemnite (VPDB) scale. All results are reported in the per mille notation relative to the international VPDB scales for $\delta^{13}C$ and $\delta^{18}O$ respectively. Stable isotope ratios are expressed as delta (δ) and are measures of a 'per mille' (‰), or parts per thousand, difference between the isotope ratio of a sample and that of a known (international) standard material. Values are reported relative to VPDB reference material for carbon and oxygen. Oxygen isotopic ratios are commonly compared to both the VSMOW[47] and the VPDB[48] references. Traditionally, oxygen in water is reported relative to VSMOW while oxygen liberated from carbonate rocks or other geologic archives is reported relative to VPDB. As in the case of hydrogen, the oxygen isotopic scale is defined by two materials, VSMOW2 and SLAP2. Measurements of sample $\delta^{18}O$ vs. VSMOW can be converted to the VPDB reference frame through the following equation: $\delta^{18}O(VPDB) = 0.97001*\delta^{18}OVSMOW - 29.99‰$.

Geochemical characterization of stone tools

Quartzite artifacts from Layer III ($n = 17$) and Layer IV ($n = 15$) in Trench 1 were selected for raw material sourcing according to stratigraphic, technological, and lithological considerations. Prior to analysis, artifacts were individually sonicated (10 minutes; 40 kHz) in glass beakers using distilled water to facilitate macroscopic classification and to prevent geochemical contamination. Artifacts were compared with a geological reference collection and classified into nine macroscopic groups, including Green1 ($n = 1$), Gray1 ($n = 12$), Gray2 ($n = 3$), Red2 ($n = 1$), Red6 ($n = 1$), White1 ($n = 10$), White2 ($n = 1$), White3 ($n = 1$), and White4 ($n = 2$).

Artifacts were geochemically characterized in a non-destructive manner by targeting the flattest surfaces to reduce X-ray scattering using a Thermo Scientific ARL QUANT'X Energy Dispersive X-ray Fluorescence spectrometer (end window bremsstrahlung; Rh target X-ray tube 50 W; 76 µm beryllium window; 4–50 kV; Edwards RV8 vacuum pump). X-ray intensities were automatically converted to concentration estimates (major oxides=wt%; trace elements=ppm) using a least-squares calibration line ratioed to the Compton scatter based on the analysis of thirteen reference standards, including AGV-2 (andesite), BCR-2 (basalt), BHVO-2 (hawaiite), BIR-1a (basalt), GSP-2 (granodiorite), JR-1 (obsidian), JR-2 (obsidian), QLO-1 (quartz latite), RGM-2 (rhyolite), SDC-1 (mica schist), STM-2 (syenite), TLM-1 (tonalite), and W-2a (diabase). The targeted elements included eight major oxides (MgO, Al_2O_3, SiO_2, K_2O, CaO, TiO_2, MnO, Fe_2O_3) and ten trace elements (Cu, Zn, Rb, Sr, Y, Zr, Nb, Ba, Pb, Th). Each analytical run included the RGM-2 reference standard to ensure instrument calibration. All major oxide and most trace element (apart from Cu and Ba) concentrations recorded for the RGM-2 reference standard were within an acceptable range relative to the recommended values.

The same cleaning methods and analytical conditions were implemented for quartzite geological samples ($n = 333$) from seven sources (Endonyo Okule, $n = 18$; Endonyo Osunyai, $n = 27$; Isilale Aratum, $n = 6$; Koonge, $n = 21$; Naibor Soit, $n = 181$; Naisiusiu, $n = 51$; and Oittii, $n = 29$), which constitute the reference collection for raw material sourcing. Geological samples were classified into twelve macroscopic groups, including Green1 ($n = 26$), Gray1 ($n = 20$), Gray2 ($n = 82$), Red1 ($n = 12$), Red2 ($n = 36$), Red3 ($n = 38$), Red4 ($n = 17$), Red5 ($n = 3$), White1 ($n = 38$), White2 ($n = 12$), White3 ($n = 35$), and White4 ($n = 14$).

Raw concentration estimates for artifacts and geological samples were normalized using the Min-Max scaling method and sorted into four macroscopic groups (Green, Gray, Red, White) for geochemical comparisons. The reader is referred to the Supplementary Text for additional information on the RGM-2 reference standard, geological reference collection, and source identification. Statistical analyses were performed using the random forest supervised machine learning algorithm in RStudio using seven packages.

Palynological methods

Thirty-one samples were processed from sandy clay, mudstone, and siltstone from Facies 2, 4, and 5, respectively, for palynological analysis following standard extraction techniques at the Geological Survey of Canada (Calgary). The process included washing, acid digestion, oxidation with Schulze's solution, and staining with Safranin O; residues were mounted with polyvinyl and liquid bioplastic. Observations of terrestrial palynomorphs of unsieved preparations were made using an Olympus BX61® transmitted light microscope with oil immersion at ×400 and ×1000 magnification. Digital images were captured using an Olympus DP72 camera and Stream Motion® software. Eighteen of the samples yielded no pollen or spores. Of the productive samples, the pollen and spore sum ranges from 2 to 1623. All samples contained microscopic charcoal. The relative abundance of pollen and spores in productive samples was calculated using a pollen sum of obligately terrestrial pollen and spores, and the abundance of microscopic charcoal and fungal spores was calculated from this sum. The stratigraphic pollen diagram was plotted using the computer program Tilia (Grimm, 1993–2001).

Phytolith analysis

Phytolith extraction was completed at the University of Calgary's Clean Room Laboratory (Tropical Archaeology Laboratory, Earth Sciences Building, 811). Detailed protocols are available through the Federated Research Data Repository (https://doi.org/10.20383/101.0123). In summary, individual sediment samples were sieved at 125 µm, from which a 3.0 g portion of sediment was taken. Clay dispersion followed: the sediment was mixed with 10 mL of 0.1% sodium hexametaphosphate $(NaPO_3)_6$, with 15-min sonication and overnight orbital shaking at 200 rpm. Samples were rinsed with previously boiled reverse osmosis deionised (RODI) water and dried over 2 days at >70 °C and then weighed. Inorganic removal consisted of the samples receiving 10 mL equal parts 3 N hydrochloric (HCl) and nitric acid (HNO_3), followed by rinsing, centrifugation at 3000 rpm, drying over 2 days at >70 °C, and weighing. Removal of organics was completed by adding 10 mL of 30% hydrogen peroxide (H_2O_2) over a hot plate (70 °C), with rinsing, drying,

and weighing. Separation of phytoliths occurred through the addition of 5 mL sodium polytungstate ($3Na_2WO_4•9WO_3•H_2O$) at specific gravity 2.4. Samples were vortexed and centrifuged at 3,000 rpm for 5 min. The resulting supernatant was transferred to new centrifuge tubes, and water was used to gradually decrease specific gravity over two additional fractions, concentrating phytoliths into the third fraction. Samples were rinsed with previously boiled RODI before two rounds of centrifugation at 4500 rpm and the final drying (>70 °C) and weighing. Of this final fraction, an aliquot of 0.001 g was transferred using a glass pipette to a microscope slide, mounted with water, and inspected fresh to allow for rotation of phytoliths for 3D classification. Microscopy was performed at ×40 using an Olympus BX51 (Olympus SC50, CellSens 2.0). Phytoliths from each sample were counted over three separate slides, each with an area of 600 mm^2. Phytolith nomenclature followed Madella and others[49], with exceptions. The total number of sediment samples processed for this study was 33, and the total number of phytoliths retrieved 112.

Faunal analysis

All faunal specimens >2 cm were analyzed through well-established faunal methods. These methods include analyses of the sample set as a whole, estimations of individual age, and taphonomic modifications as described below.

We recorded the element, taxonomic classification identified, side (left or right), portion, face, and age. Specimens were grouped into size classes, including very large (>1000 kg); large (1000–300 kg), medium (300–100 kg) as well as small (<100 kg). Relative frequencies such as the number of identified specimens (NISP), minimum number of elements (MNE), and minimum number of individuals (MNI) were used to assess and compare the relative abundance of skeletal elements and species[50,51]. We created skeletal profiles for E. N. using the Minimum Animal Units (%MAU), calculated using the MNE long bone portions represented in the assemblage. The age of the animals was estimated by the replacement and wear pattern of teeth[52], with specimens grouped as sub-adult juveniles (young and sub-adult juveniles), adults (early and late prime adults), old adults, and unknown where age could not be estimated. We grouped the age classes into the three main classes to create ternary plots[53], comparing them with other local datasets.

The complete surface of all the bones and teeth was inspected with a stereomicroscope (Opthec 120 Hz) 10−45x. The assemblage displayed various taphonomic modifications that were assessed and categorized into nutritional, subaerial, and diagenic depositional phases. Cut marks[54] in the assemblage are the dominant modification observed. Cut marks in this assemblage include slicing marks, scrape marks, and chop marks[55]. A Hirox KH 7800 microscope was used to view specimens bearing cut marks, measure the cut marks, and create cut mark profiles. Anthropogenic bone breakage was recorded in the form of percussion pits, notches, and abrasion[56]. Identified tooth marks include pits, punctures, and furrowing[57] on the cancellous tissue. Their location on the bone was noted, and their measurements were taken using digital calipers[58]. Subaerial and diagenetic damage was noted as present or absent in each of the specimens. We recorded weathering[59], trampling[60,61], abrasion[62,63], rounding[64], chemical corrosion, and dissolution.

Lithic analysis

All stone tools were weighed and measured according to their technological axis. Raw material information and techno-typological attributes were recorded in a database. Raw materials, distinguished macroscopically, included quartzite, basalt, phonolite, granitoid, and sandstone. Samples were classified into 10 technological groups: *manuports*, percussive materials, cores, core fragments, flakes, proximal fragmented flakes, distal fragmented flakes, retouched flakes, LCTs, and undetermined shatter. Cores were classified by knapping method, facets (number of surfaces exploited), and polarity (direction of exploitation from a striking platform).

The cCore reduction methods we observed encompass: (i) unifacial unipolar longitudinal: cores with a single surface exploited from a single direction; (ii) unifacial bipolar opposed: cores with a single surface exploited from two opposed directions; (iii) unifacial centripetal: cores with one surface exploited from at least three directions converging at the center; (iv) bipolar-on-anvil: albeit a knapping technique, not a method, it refers to cores with evidence of placement on a passive surface; (v) bifacial orthogonal: cores with two opposed surfaces knapped each from a single direction; (vi) bifacial centripetal: cores with two exploitation surfaces organized by a horizontal plane, each side exploited from at least three directions converging at the center; (vii) multifacial multipolar: cores with four or more surfaces exploited in four different directions.

Retouched flake analysis follows the Laplace analytical typology[65]. Data curation was done through Excel. Descriptive and multivariate statistics were conducted with the paleontological statistics software. Data used on PCA was normalized through the Z-scores formula. Inkscape Open-Source vector software was used to generate figures and graphs.

Reporting summary

Further information on research design is available in the Nature Portfolio Reporting Summary linked to this article.

Data availability

All data necessary for the conclusions of the study are provided with the Article. Geochronometric and geochemical datasets used for dating and stratigraphic correlation, as well as palaeobotanical protocols, are publicly available with the Canadian Federated Research Data Repository, with digital objects identifiers cited in pertinent places within the Article.

Received: 29 May 2024; Accepted: 19 November 2024;
Published online: 16 January 2025

References

1. Clark, D. The later pleistocene cultures of Africa. *Science* **150**, 833–847 (1965).
2. McBrearty, S. & Brooks, A. S. The revolution that wasn't: a new interpretation of the origin of modern human behavior. *J. Hum. Evol.* **39**, 453–563 (2000).
3. Roberts, P. & Stewart, B. A. Defining the 'generalist specialist' niche for Pleistocene *Homo sapiens*. *Nat. Hum. Behav*. **2**, 542–550 (2018).
4. Timmermann, A. et al. Climate effects on archaic human habitats and species successions. *Nature* **604**, 495–501 (2022).
5. Zeller, E. et al. Human adaptation to diverse biomes over the past 3 million years. *Science* **380**, 604–608 (2023).
6. Foister, T. I. F., Žliobaitė, I., Wilson, O. E., Fortelius, M. & Tallavaara, M. Homo heterogenus: variability in early Pleistocene Homo environments. *Evol. Anth.* **32**, 373–385 (2023).
7. Mercader, J. et al. Earliest Olduvai hominins exploited unstable environments ~ 2 million years ago. *Nat. Commun*. **12**, 3 (2021).
8. Mussi, M. et al. Early Homo erectus lived at high altitudes and produced both Oldowan and Acheulean tools. *Science* **382**, 713–718 (2023).
9. Kleindienst, M. R. Excavations at site JK2, Olduvai Gorge, Tanzania. *Quaternaria* **17**, 145–208 (1973).
10. Leakey, M. D., Olduvai Gorge: 5, excavations in beds III, IV, and the Masek Beds, 1968–1971 (Cambridge University Press, Cambridge, 1995).
11. Hay, R. L. Geology of the Olduvai Gorge: a study of sedimentation in a Semiarid Basin (University of California Press, Berkeley, 1976).
12. Day, M. H. & Molleson, T. I. The puzzle from JK2-A femur and a tibial fragment (O.H. 34) from Olduvai Gorge, Tanzania. *J. Hum. Evol.* **5**, 455–465 (1976).
13. Rightmire, G. P. Middle Pleistocene hominids from Olduvai Gorge, Northern Tanzania. *Amer. J Phys. Anth*. **53**, 225–241 (1980).
14. Hay, R. L. Silicate reactions in three lithofacies of a semi-arid basin, Olduvai Gorge, Tanzania. *Min. Soc. Am. Spec. Pap.* **3**, 237–255 (1970).

15. Stanistreet, I. G. et al. Changing depocentre environments of Palaeolake Olduvai and carbonates as marker horizons for hiatuses and lake-level extremes. *Palaeogeogr. Palaeoclimatol. Palaeoecol*. **560**, 110032 (2020).
16. Stanistreet, G. et al. New Olduvai Basin stratigraphy and stratigraphic concepts revealed by OGCP cores into the Palaeolake Olduvai depocentre, Tanzania. *Palaeogeogr. Palaeoclimatol. Palaeoecol*. **554**, 109751 (2020).
17. Stanistreet, I. G. et al. Palaeosalinity and palaeoclimatic geochemical proxies (elements Ti, Mg, Al) vary with Milankovitch cyclicity (1.3 to 2.0 Ma), OGCP cores, Palaeolake Olduvai, Tanzania. *Palaeogeol. Palaeoclimatol. Palaeoecol*. **546**, 109656 (2020).
18. Walker, T. R. Formation of Red Beds in modern and ancient deserts. *Geo. Soc. Am. Bull.* **78**, 353–368 (1967).
19. Van Houten, F. B. Origin of red beds a review–1961–1972. *Annu. Rev. Earth Planet. Sci.* **1**, 39–61 (1973).
20. Deino, A. L. et al. Chronostratigraphy and age modeling of Pleistocene drill cores from the Olduvai Basin, Tanzania (Olduvai Gorge Coring Project). *Palaeogeogr. Palaeoclimatol. Palaeoecol.* **571**, 109990 (2021).
21. Domínguez-Rodrigo, M. et al. First partial skeleton of a 1.34-million-year-old Paranthropus boisei from Bed II, Olduvai Gorge, Tanzania. *PLoS One*. **8**, e80347 (2013).
22. McHenry, L. J., Njau, J. K., de la Torre, I. & Pante, M. C. Geochemical "fingerprints" for Olduvai Gorge Bed II tuffs and implications for the Oldowan-Acheulean transition. *Quat. Res.* **85**, 147–158 (2016).
23. Thomas, D. S. G., Ed. Arid zone geomorphology: process, form and change in drylands (Wiley-Blackwell, 2011).
24. White, F. The vegetation of africa, a descriptive memoir to accompany the UNESCO/AETFAT/UNSO vegetation map of Africa (UNESCO, 1983).
25. Huntley, B. J. Ed. The Kuiseb environment: the development of a monitoring baseline. A report of the committee for terrestrial ecosystems. Report No. 106 South African National Scientific Programmes, (National Scientific Programmes Unit: CSIR, 1985).
26. Bolinder, K. et al. Pollen morphology of Ephedra (Gnetales) and its evolutionary implications. *Grana* **55**, 24–51 (2016).
27. Barbolini, N. et al. "Cenozoic evolution of the steppe-desert biome in Central Asia," *Sci. Adv*. **6**, eabb8227 (2020).
28. Freitag, H. & Maier-Stolte, M. The genus ephedra in NE tropical Africa. *Kew Bull.* **58**, 415–426 (2003).
29. Caveney, S., Charlet, D. A., Freitag, H., Maier-Stolte, M. & Starratt, A. N. New observations on the secondary chemistry of world Ephedra (Ephedraceae). *Am. J. Bot.* **88**, 1199–1208 (2001).
30. Ritchie, J. C. & Haynes, C. V. Holocene vegetation zonation in the Eastern Sahara. *Nature* **330**, 645–647 (1987).
31. Uno, K. T. et al. Mammal diets and paleoecology across the Oldowan-Acheulean transition at Olduvai Gorge, Tanzania from stable isotope and tooth wear analyses. *J. Hum. Evol.* **120**, 76–91 (2018).
32. Mees, F., Stoops, G., Van Ranst, E., Paepe, R. & Van Overloop, E. The nature of zeolite occurrences in deposits of the Olduvai Basin, Northern Tanzania. *Clays Clay Miner.* **53**, 659–673 (2005).
33. Eckmeier, E. & Wiesenberg, G. L. B. Short-chain *n*-alkanes (C16-20) in ancient soil are useful molecular markers for prehistoric biomass burning. *J. Arch. Sci.* **36**, 1590–1596 (2009).
34. Nicholas, C. J. et al. Stratigraphy and sedimentology of the upper cretaceous to Paleogene Kilwa Group, southern coastal Tanzania. *J. Afr. Earth Sci.* **45**, 431–466 (2006).
35. Gentry, W. & Gentry, A. Fossil Bovidae (Mammalia) of Olduvai Gorge, Tanzania. Part II, (London, 1978).
36. Pante, M. C. The larger mammal fossil assemblage from JK2, Bed III, Olduvai Gorge, Tanzania: implications for the feeding behavior of Homo erectus. *J. Hum. Evol.* **64**, 68–82 (2013).
37. Yravedra, J. Rubio-Jara, S., Courtenay, L.A. & Martos, J.A. Mammal butchery by *Homo erectus* at the Lower Pleistocene Acheulean site of Juma's Korongo 2 (JK2), bed III, Olduvai Gorge, Tanzania. *Quat. Sci. Rev*. **249**, 106612 (2020).
38. Miall, A. D. Updating uniformitarianism: Stratigraphy as just a set of 'frozen accidents. *Geo. Soc. Spec. Publ.* **404**, 11–36 (2015).
39. Dazé, A., Lee, J. K. W. & Villeneuve, M. An intercalibration study of the Fish Canyon sanidine and biotite 40Ar/39Ar standards and some comments on the age of the Fish Canyon Tuff. *Chem. Geol.* **199**, 111–127 (2003).
40. Kuiper, K. F. et al. Synchronizing rock clocks of earth history. *Science* **320**, 500–504 (2008).
41. Phillips, D., Onstott, T. C. & Harris, J. W. $^{40}Ar/^{39}Ar$ laser-probe dating of diamond inclusions from the Premier kimberlite. *Nature* **340**, 460–462 (1989).
42. Steiger, R. H. & Jager, E. Subcommission on geochronology: convention on the use of decay constants in geo-and cosmochronology compiled by. *Earth Planet. Sci. Lett.* **36**, 359–362 (1977).
43. Roddick, J. C. High precision intercalibration of 40Ar-39Ar standards. *Geochim. Cosmochim. Acta* **47**, 887–898 (1983).
44. Renne, P. R. et al. Intercalibration of standards, absolute ages and uncertainties in 40Ar/ 39Ar dating. *Chem. Geol.* **145**, 117–152 (1998).
45. Renne, P. R. & Norman, E. B. Determination of the half-life of 37Ar by mass spectrometry. *Phys. Rev. C.* **63**, 473021–473023 (2001).
46. Min, K., Mundil, R., Renne, P. R. & Ludwig, K. R. A test for systematic errors in 40 Ar/ 39 Ar geochronology through comparison with U/Pb analysis of a 1.1-Ga rhyolite. *Geochim. Cosmochim. Acta* **64**, 73–98 (2000).
47. Hut, G. Consultants' Group Meeting on stable isotope reference samples for geochemical and hydrological investigations. (International Atomic Energy Agency, Vienna, 1987).
48. Dansgaard, W. Stable isotopes in precipitation. *Tellus* **16**, 436–468 (1964).
49. Madella, M., Alexandre, A. & Ball, T. International code for phytolith nomenclature 1.0. *Ann. Bot.* **96**, 253–260 (2005).
50. Binford, L. R. Bones: ancient men and modern myths. (Academic Press, 1981).
51. Gray, J. S. Species-abundance patterns. *Symposia Br. Ecol. Soc.* **27**, 53–68 (1987).
52. Bunn, H. T. & Pickering, T. R. Methodological recommendations for ungulate mortality analyses in paleoanthropology. *Quat. Res.* **74**, 388–394 (2010).
53. Steele, T. E. & Weaver, T. D. The modified triangular graph: a refined method for comparing mortality profiles in archaeological samples. *J. Archaeol. Sci.* **29**, 317–322 (2002).
54. Potts, R. & Shipman, P. Cutmarks made by stone tools on bones from Olduvai Gorge, Tanzania. *Nature* **291**, 90–108 (1981).
55. Lyman, R. L. Quantitative units and terminology in zooarchaeology. *Am. Antiquity* **59**, 36–71 (1994).
56. Blumenschine, R. J. & Selvaggio, M. M. Percussion marks on bone surfaces as a new diagnostic of hominid behaviour. *Nature* **333**, 763–765 (1988).
57. Binford, L. R. Butchering, sharing, and the archaeological record. *J. Anthropol. Archaeol.* **3**, 235–257 (1984).
58. Andrés, M., Gidna, A. O., Yravedra, J. & Domínguez-Rodrigo, M. A study of dimensional differences of tooth marks (pits and scores) on bones modified by small and large carnivores. *Archaeol. Anthropol. Sci.* **4**, 209–219 (2012).
59. Behrensmeyer, A. K. Taphonomic and ecologic information from bone weathering. *Paleobiology* **4**, 150–162 (1978).
60. Fiorillo, A. R. Taphonomy of Hazard Homestead Quarry (Ogallala Group), Hitchcock County, Nebraska. *Contrib. Geol.* **26**, 57–97 (1988).
61. Reynard, J. P. Trampling in coastal sites: an experimental study on the effects of shell on bone in coastal sediment. *Quat. Int.* **330**, 156–170 (2014).
62. Brain, C. K. Bone weathering and the problem of bone pseudo-tools. *S. Afr. J. Sci.* **63**, 3 (1967).

63. Shipman, P. & Rose, J. Early hominid hunting, butchering, and carcass-processing behaviors: approaches to the fossil record. *J. Anthropol. Archaeol.* **2**, 57–98 (1983).
64. Olsen, S. L. & Shipman, P. Surface modification on bone: trampling versus butchery. *J. Archaeol. Sci.* **15**, 535–553 (1988).
65. Laplace, G. La typologie analytique et structurale: base rationnelle d'étude des industries lithiques et osseuses. *Colloques nationaux du CNRS* Banques de données archéologiques, 92–143 (1972).

Acknowledgements

First, the authors acknowledge the essential contributions to the knowledge presented herein by the Masai communities at Oldupai Gorge. In addition, many graduate students and colleagues helped with field logistics, permits, and archaeological excavations. The Tanzania Commission for Science and Technology and the Ministry of Natural Resources and Tourism authorized work at the site, with sample export licenses coming from the Antiquities division and the Tanzanian Executive Secretary from the Mining Commission. Our work was sponsored by the Canadian Social Sciences and Humanities Research Council under its Partnership Grant Program led by the first author/PI (J.M.). Professor Noah McLean helped with age-depth modeling. Professor Maxine Kleindienst helped contextualize her excavations from the 1960s.

Author contributions

Corresponding author J.M. provided conceptualization, formal analysis, funding acquisition, investigation, methodology, project administration, resources, supervision, visualization, writing original draft, review, and editing. P.A. provided formal analysis, investigation, methodology, visualization, review, and editing. N.B. provided resources, draft review, and editing. AC provided formal analysis, funding acquisition, investigation, methodology, resources, and review. T.C. provided funding acquisition, resources, supervision, and review. S.C. provided investigation, review, and editing. A.C.T. provided formal analysis, investigation, methodology, visualization, review, and editing. J.F. provided formal analysis, investigation, methodology, visualization, review, and editing. J.G. provided formal analysis, investigation, methodology, visualization, review, and editing. R.H. provided investigation and review. J.O.K. provided formal analysis, investigation, resources, visualization, review, and editing. H.H. provided conceptualization, formal analysis, investigation, methodology, resources, supervision, review, and editing. S.H. provided conceptualization, formal analysis, funding acquisition, investigation, methodology, resources, supervision, and review. S.L. provided conceptualization, formal analysis, investigation, methodology, resources, supervision, review, and editing. S.M. provided formal analysis, investigation, methodology, visualization, and review. A.M. provided investigation and review. A.Mw. provided investigation and review. A.O. provided investigation and review. M.P. provided conceptualization, resources, supervision, review, and editing. P.R. provided investigation, review, and editing. P.S. provided formal analysis, investigation, methodology, resources, supervision, visualization, review, and editing. A.S. provided investigation and review. R.S. provided investigation, methodology, review, and editing. M.S. provided conceptualization, formal analysis, funding acquisition, investigation, methodology, resources, supervision, review, and editing. D.S. provided methodology, visualization, review, and editing. D.M. provided investigation and review. W.Z. provided investigation and review. Corresponding author P.D. provided conceptualization, formal analysis, funding acquisition, investigation, methodology, resources, supervision, visualization, co-writing original draft, review, and editing.

Competing interests

The authors declare no competing interests.

Additional information

Supplementary information The online version contains supplementary material available at https://doi.org/10.1038/s43247-024-01919-1.

Correspondence and requests for materials should be addressed to Julio Mercader or Paul Durkin.

Peer review information *Communications Earth & Environment* thanks Gabriele Macho and the other, anonymous, reviewer(s) for their contribution to the peer review of this work. Primary Handling Editors: Jiaoyang Ruan and Carolina Ortiz Guerrero. [A peer review file is available].

Reprints and permissions information is available at http://www.nature.com/reprints

Publisher's note Springer Nature remains neutral with regard to jurisdictional claims in published maps and institutional affiliations.

[1]University of Calgary, Department of Anthropology and Archaeology, Calgary, AB, Canada. [2]Max Planck Institute of Geoanthropology, Jena, Germany. [3]Catalan Institute of Human Palaeoecology and Social Evolution (IPHES), Tarragona, Spain. [4]University of Calgary, Department of Earth, Energy and Environment, Calgary, AB, Canada. [5]University of Rovira i Virgili, Prehistory Area, Tarragona, Spain. [6]National Museums of Kenya, Nairobi, Kenya. [7]University of Queensland, School of Social Science, Brisbane, QLD, Australia. [8]University of Manitoba, Department of Earth Sciences, Winnipeg, MB, Canada. [9]McMaster University, Department of Anthropology, Hamilton, ON, Canada. [10]McMaster University, School of Earth, Environment and Society, Hamilton, ON, Canada. [11]Centro Nacional de Investigación sobre la Evolución Humana (CENIEH), Burgos, Spain. [12]University of Dar es Salaam, School of Mines and Geosciences, Dar es Salaam, Tanzania. [13]University of Dodoma, Department of History and Archaeology, Dodoma, Tanzania. [14]National Museum of Tanzania, Arusha, Tanzania. [15]Australian Research Centre for Human Evolution (ARCHE), Griffith University, Nathan, QLD, Australia. [16]Smithsonian Institution, Human Origins Program, Washington, DC, USA. [17]National Museum of Natural Sciences (CSIC), Department of Palaeobiology, Madrid, Spain. [18]LysisLogic Scientific, Inc, Calgary, AB, Canada. [19]Madrid Institute for Advanced Study, Madrid, Spain. [20]Universidad Autónoma de Madrid, Madrid, Spain. [21]Interdisciplinary Center for Archaeology and Evolution of Human Behavior (ICArEHB), Universidad do Algarve, Faro, Portugal. [22]National Museum of Ethiopia, Cultural Research Directorate, Addis Ababa, Ethiopia. ✉e-mail: mercader@ucalgary.ca; paul.durkin@umanitoba.ca